Research Article Vol. 31, No. 3 / 30 Jan 2023 / Optics Express 3651
Optics EXPRESS

Manipulation of continuous variable orbital angular momentum squeezing and entanglement by pump shaping

ZHI LI,[1,2] XULIAN GUO,[1,2] HENGXIN SUN,[1,2] KUI LIU,[1,2,*] AND JIANGRUI GAO[1,2]

[1] *State Key Laboratory of Quantum Optics and Quantum Optics Devices, Institute of Opto-Electronics, Shanxi University, Taiyuan 030006, China*
[2] *Collaborative Innovation Center of Extreme Optics, Shanxi University, Taiyuan 030006, China*
[*] *liukui@sxu.edu.cn*

Abstract: Spatially structured quantum states, such as orbital angular momentum (OAM) squeezing and entanglement, is currently a popular topic in quantum optics. The method of generating and manipulating spatial quantum states on demand needs to be explored. In this paper, we generated OAM mode squeezed states of −5.4 dB for the LG_0^{+1} mode and −5.3 dB for the LG_0^{-1} mode directly by an optical parametric oscillator (OPO) for the first time. Additionally, we demonstrated that the OAM mode squeezed and entangled states were respectively generated by manipulating the nonlinear process of the OPO by controlling the relative phase of two beams of different modes, thus making two different spatial multimode pump beams. We characterized the Laguerre-Gaussian (LG) entangled states by indirectly measuring the squeezing for the $HG_{10(45^\circ)}$ mode and $HG_{10(135^\circ)}$ mode, and directly measuring the entanglement between the LG_0^{+1} and LG_0^{-1} modes. The effective manipulation of the OAM quantum state provides a novel insight into the continuous variable quantum state generation and construction on demand for high-dimensional quantum information and quantum metrology.

1. Introduction

Structured light has proved to be important for many applications such as optical microscopy [1], optical communications [2,3], optical manipulation [4], and many other fields of optics [5,6]. As one of the most typical structured lights, Laguerre–Gaussian (LG) mode, due to its hollow intensity distribution and carrying orbital angular momentum (OAM), has been widely used in several areas, such as optical tweezers [7], optical communication [8,9], cold atom traps [10,11], the optical topological effect [12], and high-precision measurement [13,14].

The LG mode is extended from the classical to the quantum regime. The LG mode squeezed state, as a probe beam, shows good performance to enhance the precision measurements [15–17]. As is well known, the fundamental mode squeezing has been routinely applied into the ground-based gravitational wave detectors (GWD) such as the Advanced LIGO and Advanced Virgo [18,19] to surpass the shot noise limit. A squeezing of 10 dB is envisaged in the third-generation GWD such as Einstein Telescope (ET) [20]and Cosmic Explorer (CE) [21]. Except for quantum noise, the mirror thermal noise in the frequency range of around 100 Hz also primarily limites the sensitivity of the next-generation GWD. However, high-order LG mode, instead of the fundamental mode, exhibits lower thermal noise due to their more homogeneous power distributions [22,23], making the generation of high-order LG mode squeezing necessary. Meanwhile, the LG mode entanglement has potential applications into quantum information [24] and building high-capacity quantum communication networks [25,26], due to its unique capabilities in tailoring the dimensionality of the Hilbert space. Therefore, the OAM squeezing and entanglement can satisfy different application demands. The purpose of our study is to

#479583 https://doi.org/10.1364/OE.479583
Journal © 2023 Received 1 Nov 2022; revised 10 Dec 2022; accepted 22 Dec 2022; published 17 Jan 2023

develop an efficient method for generating and manipulating the spatial structure of quantum states on demand.

Optical parametric oscillator (OPO) is an important device to generate continuous variable squeezing and entanglement. Generally, the fundamental mode squeezing and entanglement can be directly generated from OPO with a fundamental mode pump beam. The fundamental mode squeezing could be transformed into an OAM squeezing through a mode converting device such as spatial light modulator (SLM), which is a commonly-used methed to generate OAM squeezing because of its programmable flexibility. Semmler et al. used a spatial light modulator (SLM) to transform the fundamental mode squeezing into LG mode squeezing [27]. Recently, arbitrary complex amplitude distributed squeezed states, including LG mode, were realized with high efficiency using a beam shaping system with two SLMs on the fundamental mode squeezed state [28]. No report on the direct generation of the LG squeezing mode using an optical parametric oscillator (OPO) has been published thus far.

For the OAM entanglement generation, Pecoraro et al. used the q-plate to convert a quantum state of a fundamental mode into the OAM entangled light [29]. However, due to the strong absorption and the unwanted diffraction of the conversion system, the quantum fields are subject to large losses and deterioration. Another method to generate the entangled state is directly using an OPO. Lassen et al. generated the quadrature entanglement of the first-order LG modes with a type I OPO in 2009 [30]. The continuous variable hyperentanglement of polarization and OAM was realized in a multimode type II OPO in 2014 [26]. However, most of the previous works adopted the fundamental mode [31] as the pump to generate the CV OAM quantum state, which has limited capability to improve the nonlinear conversion efficiency and manipulate the quantum state.

In this paper, we first produced OAM mode squeezed state of -5.4 ± 0.18 dB and -5.3 ± 0.12 dB for the LG_0^{+1} mode and the LG_0^{-1} mode respectively in type I OPO below the threshold. To the best of our knowledge, this is the highest amount of squeezing in the LG mode reported thus far. Furthermore, the LG mode squeezing was changed into LG mode entanglement by shaping the spatial structure of the pump mode. We obtained a squeezing of -5.5 ± 0.19 dB and -5.3 ± 0.17 dB for the $HG_{10(45^\circ)}$ and $HG_{10(135^\circ)}$ modes, respectively, which revealed the entanglement between the LG_0^{+1} and LG_0^{-1} modes clearly. To prove the experiment result, we directly measured the first-order LG modes entanglement using the balanced homodyne detectors (BHDs). Our study improves the nonlinear conversion efficiency and reduces the losses introduced by the optical elements. The efficient manipulation of the OAM quantum state provides a new insight into CV quantum state generation and construction on demand for high-dimensional quantum information and quantum metrology.

2. Theoretical model

A spatially tailored pump beam with a frequency of 2ω drives a type I crystal and the down-converted beams with a frequency of ω are generated from the OPO cavity. In the interaction picture, assuming perfect phase matching and exact resonance between the field and the cavity and assuming that the pump is not depleted, the interaction Hamiltonian of the system is

$$H_{\text{int}} = i\hbar\varepsilon_{pump} \sum_{k,j} \kappa_{kj}\hat{a}_k^+\hat{a}_j^+ + h.c. \tag{1}$$

Here, k and j represent the two down-converted OAM modes $LG_{p_1}^{l_1}$ and $LG_{p_2}^{l_2}$ respectively. $l_i(i = 1, 2)$ is the azimuthal index (any integers) corresponding to OAM and $p_i(i = 1, 2)$ is the radial index (zero or positive integers). $\hat{a}_k$ and $\hat{a}_j$ are the annihilation operators of the down-converted fields. ε_{pump} is the average amplitude of the pump field. κ_{kj} is the nonlinear coupling constant [32], which depends on the spatial overlap between the pump (green) and down-converted fields (red) as shown in Fig. 1.

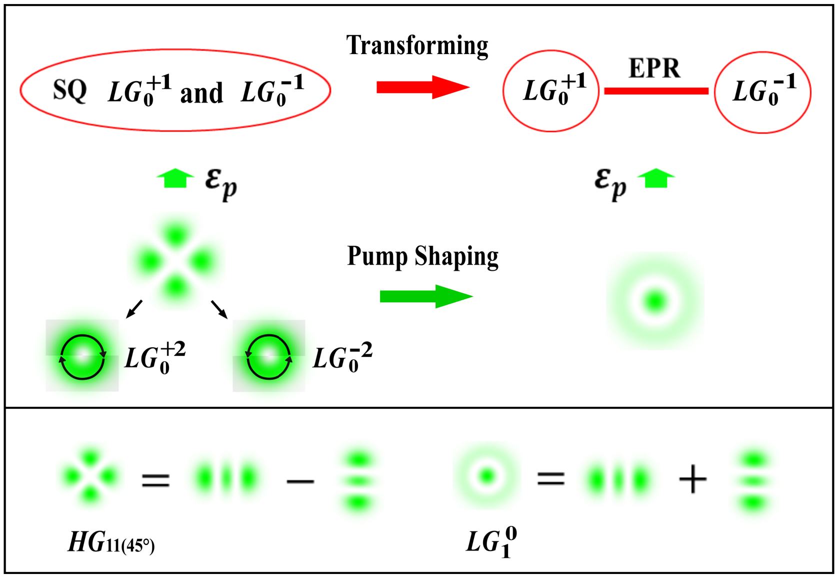

Fig. 1. Schematic illustration of the physical system. The spatially tailored pump beam ε_{pump} (green) drives an optical parametric oscillator (OPO) below the threshold, and the spatial modes of the down-conversion fields squeezed (SQ) and entangled (EPR) are generated. EPR (red line) represents the entanglement between a pair of down-conversion fields with LG modes. SQ represents the squeezing with LG modes. Pump mode LG_1^0 ($p = 1, l = 0$) and $HG_{11(45^\circ)}$ with different spatial distributions were used in the experiment and are the superpositions of HG_{20} and HG_{02}.

According to the Eq. (1), the type I OPO down-conversion processes is to meet the conservation of energy and OAM. Different pump modes correspond to different down-converted fields, thus providing a method to manipulate the generation of LG mode squeezed state and LG mode entangled state. Due to the spatial selection of the OPO cavity, the spatial modes are output with the same order. Here, we only consider the case of $|l_i| = 1$. (a) For the squeezing, the Hermite–Gaussian $HG_{11(45^\circ)}$ mode is equal to the superposition of the LG_0^{+2} and LG_0^{-2} modes. A pump photon in a LG_0^{+2} mode is annihilated in the down-conversion process, and a pair of degenerate down-converted photons are created, i.e., $l_1 = l_2 = +1$, $p_1 = p_2 = 0$ refers to LG_0^{+1} mode. Similarly, the LG_0^{-2} pump mode corresponds to the LG_0^{-1} mode squeezed state. (b) For the entanglement, once a pump photon in the LG_1^0 ($p = 1$, $l = 0$) mode is annihilated in the down-conversion process, there are two distinct possible channels in which a pair of down-converted photons are created. The two possibilities are (i) an idler photon is emitted in the LG_0^{+1} mode and a signal photon is emitted in the LG_0^{-1} mode, and (ii) a signal photon is emitted in the LG_0^{+1} mode and an idler photon is emitted in the LG_0^{-1} mode.

3. Experimental setup and results

Figure 2(a) shows our experimental setup. A continuous-wave light beam from a fiber laser at 1080 nm was split into two. One of the beams was upconverted into 540 nm by cavity-enhanced second harmonic generation (SHG). The SHG output beam passed through a mode converter MC2, which converted the HG_{00} mode into the HG_{20} mode. The HG_{20} mode was passed through a Dove prism and was converted into a HG_{02} mode. The relative phase ϕ between the HG_{20} and HG_{02} modes was locked to produce the LG_1^0 ($p = 1$, $l = 0$) mode ($\phi = 0$) and $HG_{11(45^\circ)}$ mode ($\phi = \pi$), which then drove the OPO as the pump. In our experiment, the doubly resonant OPO was kept resonant for both the 1080nm down-conversion field and the 540nm pump field. The different pump modes were resonant in the same cavity length as they have the same mode order and experience the same Gouy phase. The OPO cavity consisted of two curved mirrors (M1 and M2) of 50 mm radius of curvature and two plane mirrors (M3 and M4). A $1 \times 5 \times 12mm^3$ periodically poled potassium titanyl phosphate crystal (Raicol, Inc.) was placed in the center of two curved mirrors. Three of the four mirrors were highly reflective at 1080 nm and 540 nm, R > 99.95%, while the output coupler mirror M4 was T = 15% at 1080 nm and T = 5% at 540 nm. The squeezed and entangled states were verified using the BHD with spatially tailored local oscillators (LOs).

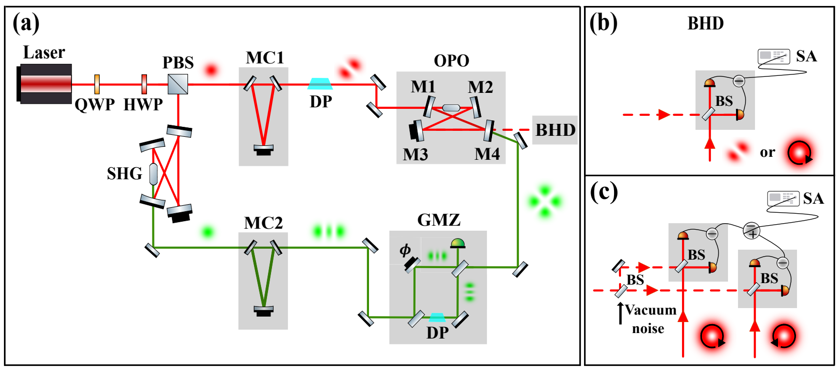

Fig. 2. Schematics of the experimental setup to generate squeezing and entanglement. Half-wave plate (HWP), quarter-wave plate (QWP), polarizing beam splitter (PBS), second harmonic generation (SHG), mode convert cavity (MC), Dove prism (DP), green Mach–Zehnder (GMZ) interferometer for the generation of the pump mode, optical parametric oscillator (OPO), balance homodyne detector (BHD), beam splitter (BS), spectrum analyzer (SA).

With the $HG_{11(45^\circ)}$ as a pump mode, the LG mode squeezing was generated. The HG_{00} mode passed through a mode converter MC1, and was converted into the HG_{10} mode. The $HG_{10(45^\circ)}$ as an auxiliary beam was generated by converting the HG_{10} mode using a Dove prism. Approximately 30 mW of the transmitted light was used as an auxiliary beam for mode matching between the down-converted beam and OPO cavity, measurement of the classical parameter gain, and adjustment of the interference efficiency between the down-converted beam and LO beam. The LO beam was a superposition of HG_{10} and HG_{01} modes, and the relative phase between the HG_{10} and HG_{01} was locked to produce the LG_0^{+1} and LG_0^{-1} modes. The measured squeezing levels were then analyzed with a spectrum analyzer as shown in Fig. 2(b). Figure 3(a) and Fig. 3(b) show the generated squeezing. We measured -5.4 ± 0.18 dB and -5.3 ± 0.12 dB of squeezing for the LG_0^{+1} and LG_0^{-1} modes, respectively. Trace 1 was the shot-noise limit (SNL), which was obtained by blocking the squeezed light. Trace 2 was the squeezing level that was normalized to the SNL. The measured efficiency of the spatial overlaps between the signal beam and LO beam was 0.97 ± 0.02, the transmitting efficiency was 0.99 ± 0.005, and the measured photodiode efficiency was 0.97 ± 0.02.

With the LG_1^0 ($p = 1$, $l = 0$) as a pump mode, the LG mode entanglement was generated. To verify the LG mode entanglement, we measured the quadrature variances for the $HG_{10(45^\circ)}$ and $HG_{10(135^\circ)}$ modes. The quadrature variances for the HG modes were analyzed using BHD with a spatially tailored LO mode, which was either a $HG_{10(45^\circ)}$ or a $HG_{10(135^\circ)}$ mode depending on the signal mode to be measured (see Fig. 2(b)). The $HG_{10(45^\circ)}$ mode squeezing level was -5.5 ± 0.19 dB for the variance $\left\langle \Delta^2 \hat{X}_{HG_{10(45^\circ)}} \right\rangle = 0.28 \pm 0.01$, the $HG_{10(135^\circ)}$ mode squeezing level was -5.3 ± 0.17 dB for the variance $\left\langle \Delta^2 \hat{X}_{HG_{10(135^\circ)}} \right\rangle = 0.30 \pm 0.01$, as shown in Fig. 3(c) and

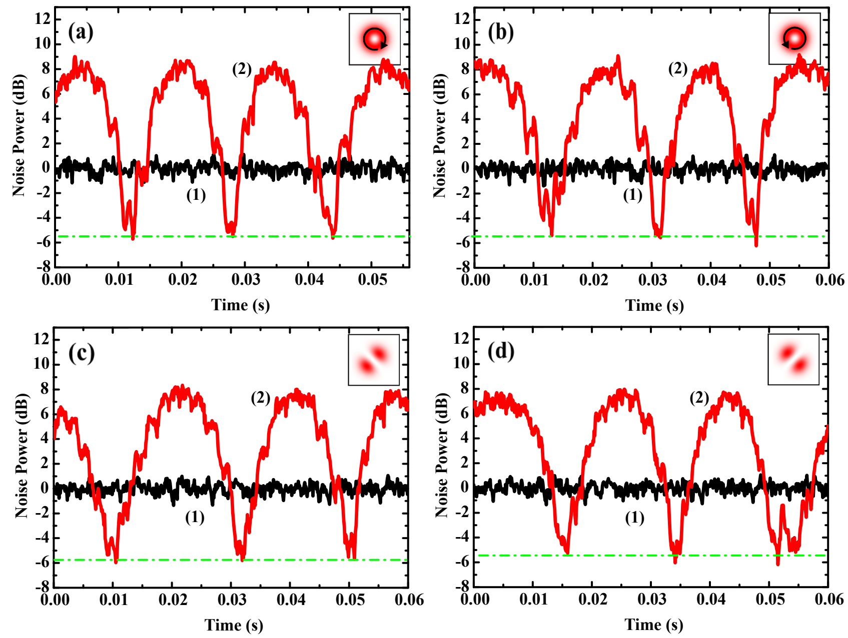

Fig. 3. Experimental results of the squeezed state with different local mode. Trace 1 (black line): SNL. (a) Trace 2 (red line): the measured squeezing for the LG_0^{+1} mode with LG_0^{+1} local mode. (b) Trace 2 (red line): the measured squeezing for the LG_0^{-1} mode with LG_0^{-1} local mode. (c) Trace 2 (red line): the measured squeezing for the $HG_{10(45°)}$ mode with $HG_{10(45°)}$ local mode. (d) Trace 2 (red line): the measured squeezing for the $HG_{10(135°)}$ mode with $HG_{10(135°)}$ local mode. The measurement parameters for the spectrum analyzer are RBW (300 kHz) and VBW (470 Hz), and the analysis frequency is 3 MHz.

Fig. 3(d). Trace 1 and trace 2 were respectively the SNL and the correlation variance that was normalized to SNL.

By performing a basis transformation from the HG modes to the LG modes, we have

$$\hat{X}_{HG_{10(45°)}} = (\hat{X}_{HG_{10}} + \hat{X}_{HG_{01}})\Big/\sqrt{2}, \tag{2}$$

$$\hat{X}_{HG_{10(135°)}} = (\hat{X}_{HG_{10}} - \hat{X}_{HG_{01}})\Big/\sqrt{2}, \tag{3}$$

$$\hat{X}_{HG_{10}} = (\hat{X}_{LG_0^{+1}} + \hat{X}_{LG_0^{-1}})\Big/\sqrt{2}, \tag{4}$$

$$\hat{X}_{HG_{01}} = (\hat{P}_{LG_0^{+1}} - \hat{P}_{LG_0^{-1}})\Big/\sqrt{2}. \tag{5}$$

Here, $\hat{X}$ and $\hat{P}$ are the amplitude and phase quadrature, respectively. $\hat{X}_{LG_p^l} = \frac{1}{\sqrt{2}}(\hat{a}_{LG_p^l} + \hat{a}^+_{LG_p^l})$ is the amplitude quadrature and $\hat{P}_{LG_p^l} = \frac{1}{\sqrt{2}i}(\hat{a}_{LG_p^l} - \hat{a}^+_{LG_p^l})$ is the phase quadrature. The inseparability criterion of the entanglement is given by [33,34]

$$\left\langle \Delta^2(\hat{X}_{LG_0^{+1}} + \hat{X}_{LG_0^{-1}})\right\rangle + \left\langle \Delta^2(\hat{P}_{LG_0^{+1}} - \hat{P}_{LG_0^{-1}})\right\rangle < 2. \tag{6}$$

From Eqs. (2) to (5), we get

$$\left\langle \Delta^2\hat{X}_{HG_{10(45°)}}\right\rangle + \left\langle \Delta^2\hat{X}_{HG_{10(135°)}}\right\rangle = \left\langle \Delta^2(\hat{X}_{LG_0^{+1}} + \hat{X}_{LG_0^{-1}})\right\rangle + \left\langle \Delta^2(\hat{P}_{LG_0^{+1}} - \hat{P}_{LG_0^{-1}})\right\rangle. \tag{7}$$

Optics EXPRESS

Using the transformation, the criterion reduces to $\langle \Delta^2 \hat{X}_{HG_{10(45^\circ)}} \rangle + \langle \Delta^2 \hat{X}_{HG_{10(135^\circ)}} \rangle < 2$. The entanglement between the LG_0^{+1} and LG_0^{-1} modes can be witnessed by measuring the quadrature variances of the $HG_{10(45^\circ)}$ and $HG_{10(135^\circ)}$ modes.

Thus, we have

$$\langle \Delta^2 \hat{X}_{HG_{10(45^\circ)}} \rangle + \langle \Delta^2 \hat{X}_{HG_{10(135^\circ)}} \rangle = 0.58 \pm 0.01 < 2, \tag{8}$$

which shows the entanglement between the signal modes LG_0^{+1} and LG_0^{-1} clearly.

We also directly measured the entanglement by two pairs of BHDs as shown in Fig. 2(c). Similarly, using the LG_1^0 mode as the pump, the correlation variances for LG_0^{+1} and LG_0^{-1} modes were obtained by BHDs at the analysis frequency of 3 MHz. As shown in Fig. 4, trace 1 was SNL and trace 2 was the correlation variance normalized to SNL. Figure 4(a) shows the anti-squeezing of 3.8 ± 0.16 dB for the sum of phase quadratures $\left\langle \Delta^2(\hat{P}^m_{LG_0^{+1}} + \hat{P}^m_{LG_0^{-1}}) \right\rangle$ (trace 3) and the squeezing of -1.8 ± 0.12 dB for the difference of phase quadratures $\left\langle \Delta^2(\hat{P}^m_{LG_0^{+1}} - \hat{P}^m_{LG_0^{-1}}) \right\rangle$ (trace 4). Figure 4(b) shows the anti-squeezing of 3.2 ± 0.12 dB for the difference of amplitude quadratures $\left\langle \Delta^2(\hat{X}^m_{LG_0^{+1}} - \hat{X}^m_{LG_0^{-1}}) \right\rangle$ (trace 3), and the squeezing of -1.7 ± 0.10 dB for the sum of amplitude quadratures $\left\langle \Delta^2(\hat{X}^m_{LG_0^{+1}} + \hat{X}^m_{LG_0^{-1}}) \right\rangle$ (trace 4). The small difference between the sum of amplitude quadratures and the difference of phase quadratures was due to the existence of the additional noise [35]. Thus, we have

$$\left\langle \Delta^2(\hat{X}^m_{LG_0^{+1}} + \hat{X}^m_{LG_0^{-1}}) \right\rangle + \left\langle \Delta^2(\hat{P}^m_{LG_0^{+1}} - \hat{P}^m_{LG_0^{-1}}) \right\rangle = 1.34 \pm 0.02 < 2, \tag{9}$$

which clearly shows the entanglement between the signal modes LG_0^{+1} and LG_0^{-1}.

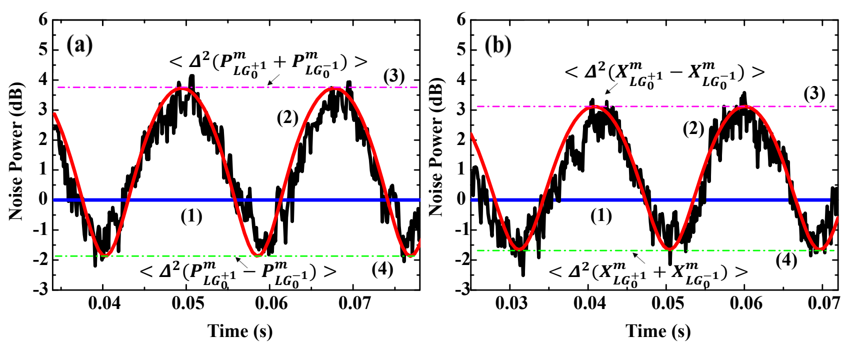

Fig. 4. Experimental results of entanglement. Trace 1 (blue line): SNL. Trace 2 (black line): the correlation variance for LG_0^{+1} and LG_0^{-1} modes. (a) Trace 3 (pink line): the sum of phase quadratures $\left\langle \Delta^2(\hat{P}^m_{LG_0^{+1}} + \hat{P}^m_{LG_0^{-1}}) \right\rangle$; trace 4 (green line): the difference of phase quadratures $\left\langle \Delta^2(\hat{P}^m_{LG_0^{+1}} - \hat{P}^m_{LG_0^{-1}}) \right\rangle$. (b) Trace 3 (pink line): the difference of amplitude quadratures $\left\langle \Delta^2(\hat{X}^m_{LG_0^{+1}} - \hat{X}^m_{LG_0^{-1}}) \right\rangle$; trace 4 (green line): the sum of amplitude quadratures $\left\langle \Delta^2(\hat{X}^m_{LG_0^{+1}} + \hat{X}^m_{LG_0^{-1}}) \right\rangle$. The measurement parameters for the spectrum analyzer are RBW (300 kHz) and VBW (470 Hz), and the analysis frequency is 3 MHz.

However, vacuum noise was introduced by the beam splitter in the above experimental setup. Introducing vacuum field, the measured field with the BHD (see Fig. 2(c)) of the entangled state

Optics EXPRESS

can be written as

$$\hat{a}^{m}_{LG_0^{+1}} = \frac{1}{\sqrt{2}}(\hat{a}_{LG_0^{+1}} + \hat{a}^{v}_{LG_0^{+1}}), \tag{10}$$

$$\hat{a}^{m}_{LG_0^{-1}} = \frac{1}{\sqrt{2}}(\hat{a}_{LG_0^{-1}} - \hat{a}^{v}_{LG_0^{-1}}). \tag{11}$$

Here, $\hat{a}^{m}_{LG_0^{\pm1}}$, $\hat{a}_{LG_0^{\pm1}}$ and $\hat{a}^{v}_{LG_0^{\pm1}}$ are the annihilation operator describing measured field, OPO direct output field and vacuum field.

According to Eqs. (10) and (11), the sum of amplitude quadratures describing OPO direct output field can be inferred:

$$\left\langle \Delta^2(\hat{X}_{LG_0^{+1}} + \hat{X}_{LG_0^{-1}})\right\rangle = 2\left\langle \Delta^2(\hat{X}^{m}_{LG_0^{+1}} + \hat{X}^{m}_{LG_0^{-1}})\right\rangle - 1 = 0.35. \tag{12}$$

Similarly, the difference of phase quadratures describing OPO direct output field is

$$\left\langle \Delta^2(\hat{P}_{LG_0^{+1}} - \hat{P}_{LG_0^{-1}})\right\rangle = 2\left\langle \Delta^2(\hat{P}^{m}_{LG_0^{+1}} - \hat{P}^{m}_{LG_0^{-1}})\right\rangle - 1 = 0.32. \tag{13}$$

Thus, we have

$$\left\langle \Delta^2(\hat{P}_{LG_0^{+1}} - \hat{P}_{LG_0^{-1}})\right\rangle + \left\langle \Delta^2(\hat{X}_{LG_0^{+1}} + \hat{X}_{LG_0^{-1}})\right\rangle = 0.67 < 2. \tag{14}$$

The inferred correlation variance was almost consistent with the result of the first method ($\langle \Delta^2 \hat{X}_{HG_{10(45^\circ)}}\rangle + \langle \Delta^2 \hat{X}_{HG_{10(135^\circ)}}\rangle = 0.58 \pm 0.01 < 2$). In fact, the coupled vacuum noise could be avoided by the direct separation of the two entangled LG modes with an interferometer shown in Ref. [36].

The measured correlations were degraded by the various inefficiencies during the measuring process. The total measuring efficiency is expressed as $\eta_{to} = \eta_{tr} \cdot \eta_{qu} \cdot \eta^2_{hd}$, where $\eta_{tr} = 0.98 \pm 0.01$ is the transmitting efficiency, $\eta_{qu} = 0.97 \pm 0.02$ is the quantum efficiency of the photodiode, and $\eta_{hd} = 0.97 \pm 0.02$ is the interference visibility between the signal and LO beams, both for HG_{00} modes. The measuring efficiency for the total detection is $\eta_{tol} = 0.89 \pm 0.03$.

4. Conclusion

We implemented the manipulation of the CV OAM mode squeezing and entanglement by shaping the pump beam profile of the OPO. We experimentally generated the LG mode squeezed state in the OPO below the threshold with, to our knowledge, the highest amount of squeezing in the LG mode reported thus far. This technique holds promise for applications into spatial measurements [15,16]. Besides, the quantum technique may be extended to higher-order LG mode squeezed states to enhance the sensitivity of gravitational-wave detection [23]. The squeezing level is mainly limited by the pump power and intracavity loss for the current system. In our next work, we will optimize the experimental system by using high efficiency beam shaping devices to increase the optical pump power and designing the OPO cavity with lower internal cavity loss, thus possibly to obtain squeezing greater than 10 dB. In addition, an effective method for manipulating the CV OAM quantum state was achieved, which resulted in reduced losses from optical devices outside the cavity. Therefore, it is much easier to prepare entanglement between two orthogonal spatial modes within one beam by simplifying the experiment setup for the application into optical multi-mode quantum communication systems [31,37].

Funding. National Key Research and Development Program of China (2021YFC2201802); Shanxi (1331 Project); Shanxi Scholarship Council of China (2021-05); National Natural Science Foundation of China (12074233).

Disclosures. The authors declare no conflicts of interest.

Optics EXPRESS

Data availability. Data that support the findings of this study are available from the corresponding authors upon reasonable request.

References

1. C. Maurer-Grubinger, A. Jesacher, S. Bernet, and M. Ritsch-Marte, "What spatial light modulators can do for optical microscopy," Laser Photonics Rev. **5**(1), 81–101 (2011).
2. N. Gisin and R. Thew, "Quantum communication," Nat. Photonics **1**(3), 165–171 (2007).
3. X.-L. Wang, X.-D. Cai, Z.-E. Su, M.-C. Chen, D. Wu, L. Li, N.-L. Liu, C.-Y. Lu, and J.-W. Pan, "Quantum teleportation of multiple degrees of freedom of a single photon," Nature **518**(7540), 516–519 (2015).
4. D. Grier, "A revolution in optical manipulation," Nature **424**(6950), 810–816 (2003).
5. H. Rubinsztein-Dunlop, A. Forbes, and M. Berry, *et al.*, "Roadmap on structured light," J. Opt. **19**(1), 013001 (2017).
6. A. Forbes, M. de Oliveira, and M. R. Dennis, "Structured light," Nat. Photonics **15**(4), 253–262 (2021).
7. A. Ashkin, J. Dziedzic, J. Bjorkholm, and S. Chu, "Observation of a single-beam gradient force optical trap for dielectric particles," Opt. Lett. **11**(5), 288–290 (1986).
8. N. Bozinovic, Y. Yue, Y. Ren, M. Tur, P. Kristensen, H. Huang, A. Willner, and S. Ramachandran, "Terabit-scale orbital angular momentum mode division multiplexing in fibers," Science **340**(6140), 1545–1548 (2013).
9. R. C. Devlin, N. A. Rubin, J. P. Balthasar Mueller, and F. Capasso, "Arbitrary spin-to-orbital angular momentum conversion of light," Science **358**(6365), 896–901 (2017).
10. M. F. Andersen, C. Ryu, P. Cladé, V. Natarajan, A. Vaziri, K. Helmerson, and W. D. Phillips, "Quantized rotation of atoms from photons with orbital angular momentum," Phys. Rev. Lett. **97**(17), 170406 (2006).
11. K. C. Wright, L. S. Leslie, and N. P. Bigelow, "Optical control of the internal and external angular momentum of a bose-einstein condensate," Phys. Rev. A **77**(4), 041601 (2008).
12. K. Y. Bliokh and F. Nori, "Transverse and longitudinal angular momenta of light," Phys. Rep. **592**, 1–38 (2015).
13. J. Arlt, M. Macdonald, L. Paterson, W. Sibbett, K. Dholakia, and K. Volke-Sepulveda, "Moving interference patterns created using the angular doppler-effect," Opt. Express **10**(16), 844–852 (2002).
14. M. Lavery, F. Speirits, S. Barnett, and M. Padgett, "Detection of a spinning object using light's orbital angular momentum," Science **341**(6145), 537–540 (2013).
15. K. Liu, C. Cai, J. Li, L. Ma, H. Sun, and J. Gao, "Squeezing-enhanced rotating-angle measurement beyond the quantum limit," Appl. Phys. Lett. **113**(26), 261103 (2018).
16. V. D'Ambrosio, N. Spagnolo, L. Del Re, S. Slussarenko, Y. Li, L. Kwek, L. Marrucci, S. Walborn, L. Aolita, and F. Sciarrino, "Photonic polarization gears for ultra-sensitive angular measurements," Nat. Commun. **4**(1), 2432 (2013).
17. O. Magana-Loaiza, M. Mirhosseini, B. Rodenburg, and R. Boyd, "Amplifcation of angular rotations using weak measurements," Phys. Rev. Lett. **112**(20), 200401 (2014).
18. M. Tse, H. Yu, and N. Kijbunchoo, *et al.*, "Quantum-Enhanced Advanced LIGO Detectors in the Era of Gravitational-Wave Astronomy," Phys. Rev. Lett. **123**(23), 231107 (2019).
19. F. Acernese, M. Agathos, and L. Aiello, *et al.*, "Quantum backaction on kg-scale mirrors: Observation of radiation pressure noise in the advanced virgo detector," Phys. Rev. Lett. **125**(13), 131101 (2020).
20. M. Punturo, M. Abernathy, and F. Acernese, *et al.*, "The einstein telescope: A third-generation gravitational wave observatory," Class. Quantum Grav. **27**(19), 194002 (2010).
21. D. Reitze, R. Adhikari, and S. Ballmer, *et al.*, "Cosmic Explorer: The U.S. contribution to gravitational-wave astronomy beyond LIGO," Bull. Am. Astron. Soc. **51**, 035 (2019).
22. S. Chelkowski, S. Hild, and A. Freise, "Prospects of higher-order laguerre-gauss modes in future gravitational wave detectors," Phys. Rev. D **79**(12), 122002 (2009).
23. R. Schnabel, N. Mavalvala, D. E. McClelland, and P. K. Lam, "Quantum metrology for gravitational wave astronomy," Nat. Commun. **1**(1), 121 (2010).
24. K. Liu, J. Guo, C. Cai, S. Guo, and J. Gao, "Experimental generation of continuous-variable hyperentanglement in an optical parametric oscillator," Phys. Rev. Lett. **113**(17), 170501 (2014).
25. W. Wang, K. Zhang, and J. Jing, "Large-scale quantum network over 66 orbital angular momentum optical modes," Phys. Rev. Lett. **125**(14), 140501 (2020).
26. S. Li, X. Pan, Y. Ren, H. Liu, S. Yu, and J. Jing, "Deterministic generation of orbital-angular-momentum multiplexed tripartite entanglement," Phys. Rev. Lett. **124**(8), 083605 (2020).
27. M. Semmler, S. Berg-Johansen, V. Chille, C. Gabriel, P. Banzer, A. Aiello, C. Marquardt, and G. Leuchs, "Single-mode squeezing in arbitrary spatial modes," Opt. Express **24**(7), 7633–7642 (2016).
28. L. Ma, H. Guo, H. Sun, K. Liu, B. Su, and J. Gao, "Generation of squeezed states of light in arbitrary complex amplitude transverse distribution," Photonics Res. **8**(9), 1422–1427 (2020).
29. A. Pecoraro, F. Cardano, L. Marrucci, and A. Porzio, "Continuous-variable entangled states of light carrying orbital angular momentum," Phys. Rev. A **100**(1), 012321 (2019).
30. M. Lassen, G. Leuchs, and U. L. Andersen, "Continuous variable entanglement and squeezing of orbital angular momentum states," Phys. Rev. Lett. **102**(16), 163602 (2009).
31. J. Janousek, K. Wagner, J.-F. Morizur, N. Treps, P. K. Lam, C. Harb, and H.-A. Bachor, "Optical entanglement of co-propagating modes," Nat. Photonics **3**(7), 399–402 (2009).
32. C. Navarrete-Benlloch, G. J. de Valcárcel, and E. Roldán, "Generating highly squeezed hybrid laguerre-gauss modes in large-fresnel-number degenerate optical parametric oscillators," Phys. Rev. A **79**(4), 043820 (2009).

33. L.-M. Duan, G. Giedke, J. I. Cirac, and P. Zoller, "Inseparability criterion for continuous variable systems," Phys. Rev. Lett. **84**(12), 2722–2725 (2000).
34. R. Simon, "Peres-horodecki separability criterion for continuous variable systems," Phys. Rev. Lett. **84**(12), 2726–2729 (2000).
35. J. E. S. César, A. S. Coelho, K. N. Cassemiro, A. S. Villar, M. Lassen, P. Nussenzveig, and M. Martinelli, "Extra phase noise from thermal fluctuations in nonlinear optical crystals," Phys. Rev. A **79**(6), 063816 (2009).
36. J. Guo, C. Cai, L. Ma, K. Liu, H. Sun, and J. Gao, "Measurement of stokes-operator squeezing for continuous-variable orbital angular momentum," Sci. Rep. **7**(1), 4434 (2017).
37. R. B. Rodrigues, G. B. Alves, R. F. Barros, C. E. R. Souza, and A. Z. Khoury, "Generalized orbital angular momentum symmetry in parametric amplification," Phys. Rev. A **105**(1), 013510 (2022).